On the Detection of Continental Shelf Waves

WILLIAM W. HSIEH[1]

Department of Oceanography, University of British Columbia, Vancouver, B.C., Canada V6T 1W5

(Manuscript received 22 September 1981, in final form 16 February 1982)

ABSTRACT

Given equal amounts of kinetic energy near the coast, different shelf wave modes (at the same frequency) have different magnitudes of sea-level oscillations—the magnitudes decrease with increasing mode number. Hence, an intrinsic bias for the lowest mode is present when using sea-level data for shelf wave detection.

Shelf waves have many modal-dependent structures in their cross-shelf dimension, which can be used to accurately identify the excited modes in the current fluctuations. In addition to rotary spectral analysis, a new technique that involves fitting (at a particular frequency of interest) the theoretical current ellipses of various barotropic shelf wave modes to the observed current ellipses at stations spread across the continental shelf, is introduced. This technique shows how the current energy is distributed among the modes.

These techniques are illustrated using Oregon shelf data from the summer of 1973. The cross-shelf fitting shows that at frequencies below 0.45 cycles day^{-1}, the current fluctuations on the Oregon shelf were completely dominated by the second mode. Furthermore, the observed alongshore phase speed also agreed very closely with the theoretical value for the second mode shelf wave. This is the clearest shelf wave identification achieved to date.

1. Introduction

Within the last decade, there have been numerous observations of continental shelf waves in various parts of the world. Mooers and Smith (1968), Cutchin and Smith (1973), Huyer *et al.* (1975), Kundu *et al.* (1975), Kundu and Allen (1976), Wang and Mooers (1977), Osmer and Huyer (1978), and Huyer *et al.* (1978), are some of the papers on shelf wave observations off the west coast of North America; while Mysak and Hamon (1969), Schott and Düing (1976), Brooks and Mooers (1977) and Brooks (1978), are studies on the east coast.

Shelf waves were detected from horizontal current velocity measurements and from sea-level measurements. However, as the potential to horizontal kinetic energy ratio varies widely between different shelf wave modes, the resulting picture from spectral analysis using sea-level data can be entirely different from that using current data.

As an example, let us take the Oregon shelf, and suppose that at a frequency of ~0.13 cpd (cycles per day), the first and the second shelf wave modes are both excited, each having an alongshore velocity of 1 cm s^{-1} at the coast. However, the corresponding sea-level displacements at the coast (as illustrated by the top two diagrams in Fig. 4a) are not equal for the two modes, but have the amplitudes 0.35 and 0.11 cm—i.e., for the same current velocity at the coast, the sea-level displacement associated with the first mode is larger than that of the second mode by more than a factor of 3. When one computes the auto- or cross-spectra of sea levels, this factor is squared, resulting in the first mode appearing 10 times stronger than the second.

Now imagine a situation where the current energy of the second mode dominates over that of the first mode by a ratio of 4:1 near the coast. Due to the factor of 10 bias, the sea-level auto- and cross-spectra would nevertheless be overridden by the first mode! This scenario indeed appears to have occurred on the Oregon shelf during the summer of 1973, where Kundu and Allen (1976), using current data, deduced the alongshore propagation speed to be ~120 km day^{-1}, consistent with the second mode shelf wave, while Wang and Mooers (1977, Fig. 6b), using sea-level data, obtained a phase speed of 460 km day^{-1}, comparable to that of the first mode.

As shelf waves are basically horizontal current oscillations, the corresponding sea-level vibrations are only a secondary characteristic. Unfortunately, with current meter measurements unavailable until about a decade ago, many of the past shelf wave observations were made with sea-level data, thereby containing the strong bias for the lowest mode.

The main purpose of this paper is to introduce superior techniques for shelf-wave detection. Despite the increasing number of shelf-wave observations, the detection technique remains little changed from

[1] Present affiliation: Department of Applied Mathematics and Theoretical Physics, University of Cambridge, Cambridge CB3 9EW, England.

0022-3670/82/050414-14$07.50
© 1982 American Meteorological Society

Unauthenticated | Downloaded 12/07/23 08:32 PM UTC

that used in the first observation by Hamon (1962). The "standard" procedure involves: 1) finding a peak at angular frequency ω in the coherence spectrum between two stations separated in the alongshore direction, 2) deducing the corresponding wave-number k from the alongshore phase lag, and 3) trying to determine if the observed (k, ω) values lie close to a particular shelf-wave dispersion curve on the dispersion diagram. Little observational study has been made of the *cross-shelf* (offshore) structure.

Ironically, to the shelf-wave theorists, the interesting dimension is the cross-shelf dimension. Under the common assumption of the topography changing only in the offshore x direction, the alongshore structure of a shelf wave is a plain $\exp[i(ky - \omega t)]$, whereas the cross-shelf structure is governed by an ordinary differential equation in x. As will be illustrated in Section 2, the solution of the equation reveals a richly structured cross-shelf dimension—alternating zones of predominantly clockwise and anticlockwise motion, modal dependent energy fall-off rates, and varying shapes and orientations of the current ellipses (see Figs. 4, 5). As these cross-shelf features are unique to each mode, they provide a set of "fingerprints" for accurate modal identification.

The lack of cross-shelf observational studies is partly due to the much greater difficulties involved in mooring arrays across the continental shelf than in deploying tidegauges and current meters along the coastline. Yet, since the last decade, the desire to understand coastal upwelling phenomena has motivated the mooring of extensive cross-shelf arrays, (e.g., the CUE-1 and CUE-2 arrays on the Oregon shelf during the summers of 1972 and 1973). The data from these arrays provide a remarkable opportunity to study shelf waves from a hitherto nearly unexplored dimension.

This paper advances the theme—that shelf waves can be detected by examining the cross-shelf dimension—with the support of two techniques. First, rotary spectral analysis is performed to gain a general picture. Then, at specific frequencies, the theoretically computed shelf-wave curves for various modes (e.g. Fig. 4) are fitted across the shelf by the least-squares method to the observed current data, to determine which modes are excited. Data collected from the Oregon shelf during the CUE-2 experiment (July–August, 1973) are used to illustrate these two techniques. In a subsequent paper, more seasonal and spatial coverage is obtained by examining additional data sets (Oregon and Washington, summer 1972; and Oregon, winter and spring, 1975). The emphasis of this paper is on shelf-wave detection and identification, whereas the following paper, Hsieh (1982), focuses primarily on the findings on the Oregon and Washington shelves, upon application of these techniques. Both papers originated from the doctoral thesis of Hsieh (1981).

The outline of this paper is as follows: Section 2 examines the theoretical cross-shelf structure of the shelf waves. Section 3 introduces the cross-shelf modal fitting technique. Oregon shelf data from the summer of 1973 are analyzed by rotary spectral methods in Section 4, and by the cross-shelf fitting technique in Section 5. Section 6 discusses the limitations and possible extensions of the fitting technique. Problems with detecting shelf-waves from sea-level data are examined in Section 7, followed by a summary.

2. Cross-shelf structure of shelf waves

We start with the linearized, unforced, barotropic long-wave equations for a rotating system,

$$\tilde{u}_t - \tilde{v} = -\tilde{\eta}_x , \tag{2.1}$$

$$\tilde{v}_t + \tilde{u} = -\tilde{\eta}_y , \tag{2.2}$$

$$(h\tilde{u})_x + (h\tilde{v})_y = -\mu^2\tilde{\eta}_t , \tag{2.3}$$

where t is the time, x the offshore coordinate and y the alongshore coordinate; $(\tilde{u}, \tilde{v})$ are the horizontal velocity components in the (x, y) direction, $\tilde{\eta}$ the sea-surface displacement from equilibrium, h the depth of the ocean, and the equations have been nondimensionalized as in Hsieh and Mysak (1980). The length scale is the shelf/slope width (120 km), and the time scale is f^{-1}, where f is the Coriolis parameter. The divergence parameter μ^2 is $\simeq 0.05$ at midlatitudes.

Following Cutchin and Smith (1973), we let

$$(\tilde{u}, \tilde{v}, \tilde{\eta}) = \mathrm{Re}\{[u(x), v(x), \eta(x)]e^{i(ky-\omega t)}\}. \tag{2.4}$$

Eqs. (2.1)–(2.3) yield

$$u = i(-\omega\eta' + k\eta)(\omega^2 - 1)^{-1}, \tag{2.5}$$

$$v = (\omega k\eta - \eta')(\omega^2 - 1)^{-1}, \tag{2.6}$$

$$(h\eta')' + \left[-k^2h - \frac{k}{\omega}h' + \mu^2(\omega^2 - 1)\right]\eta = 0. \tag{2.7}$$

The dispersion curves are obtained numerically from (2.7) (with the boundary condition $hu = 0$ at $x = 0$), by a "shooting" method based on that of Caldwell and Longuet-Higgins (1971). From the numerical integration, $\eta(x)$ and $\eta'(x)$, and hence $u(x)$, $v(x)$ are known.

Fig. 1 shows the CUE-2 moorings deployed on the Oregon shelf during July–August 1973. Fig. 2a shows the topography along the cross-shelf array, while Fig. 2b displays the corresponding dispersion curves.

Introduce the complex velocity $w = \tilde{u} + i\tilde{v}$. A passing wave of angular frequency ω can be represented as a sum of anticlockwise and clockwise rotating components,

$$w = w_A + w_C = Ae^{i(\omega t+\phi)} + Ce^{-i(\omega t+\theta)}, \tag{2.8}$$

Unauthenticated | Downloaded 12/07/23 08:32 PM UTC

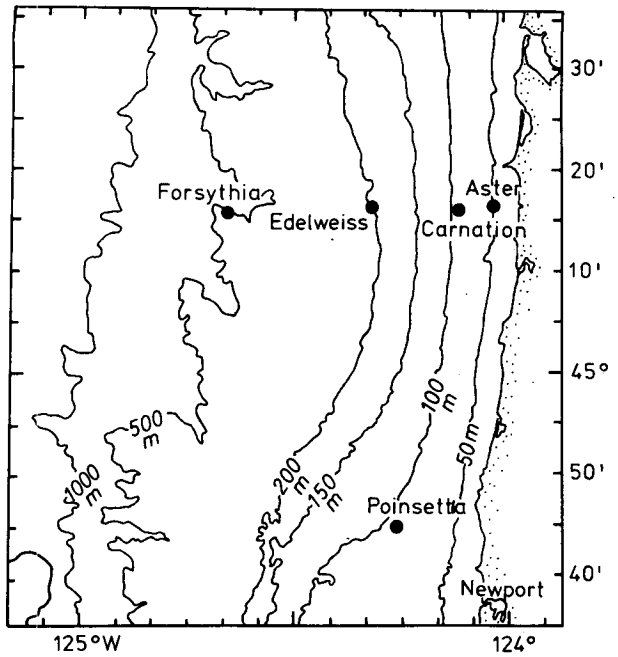

FIG. 1. Location of current meter moorings used in this study. The moorings were part of the CUE-2 array deployed on the Oregon shelf during July–August, 1973. Redrawn from Pillsbury *et al.* (1974).

where A and C are, respectively, the length of the anticlockwise and clockwise rotating vectors. At $t = 0$, the anticlockwise (clockwise) vector makes an angle ϕ ($-\theta$) with the x-axis. Fig. 3 shows the current ellipse traced out by the tip of the velocity vector. The overall rotation of the velocity vector is anticlockwise if $A > C$, and clockwise if $C > A$. The angle $\alpha = \frac{1}{2}(\phi - \theta)$ gives the direction of the major axis.

Combining (2.4)–(2.6) with (2.8), we obtain

$$A = \tfrac{1}{2}|u - iv|, \quad C = \tfrac{1}{2}|u + iv|. \qquad (2.9)$$

Hsieh (1981) showed that

$$\alpha = \begin{cases} 90° & \text{if } |\eta| < |\eta'/k| \\ 0° & \text{if } |\eta| > |\eta'/k| \end{cases}. \qquad (2.10)$$

Hence the major axis of a shelf-wave current ellipse is oriented either parallel or perpendicular to the coast.

Fig. 4a shows $u(x)$, $v(x)$ and $\eta(x)$ for five selected shelf waves, which are indicated on the dispersion diagram, Fig. 2b. The first three waves are the first, second and third modes at the frequency 0.13 cpd; while the fourth and fifth waves are both first mode waves at 0.63 cpd, but of different wavelengths. Note that for the same velocity at the coast, the corresponding sea-level displacements are very different for the five waves. In general, the sea-level displacements become smaller as the mode number increases, and as the wavelength decreases. Hence, as mentioned in the Introduction, it is very difficult to detect

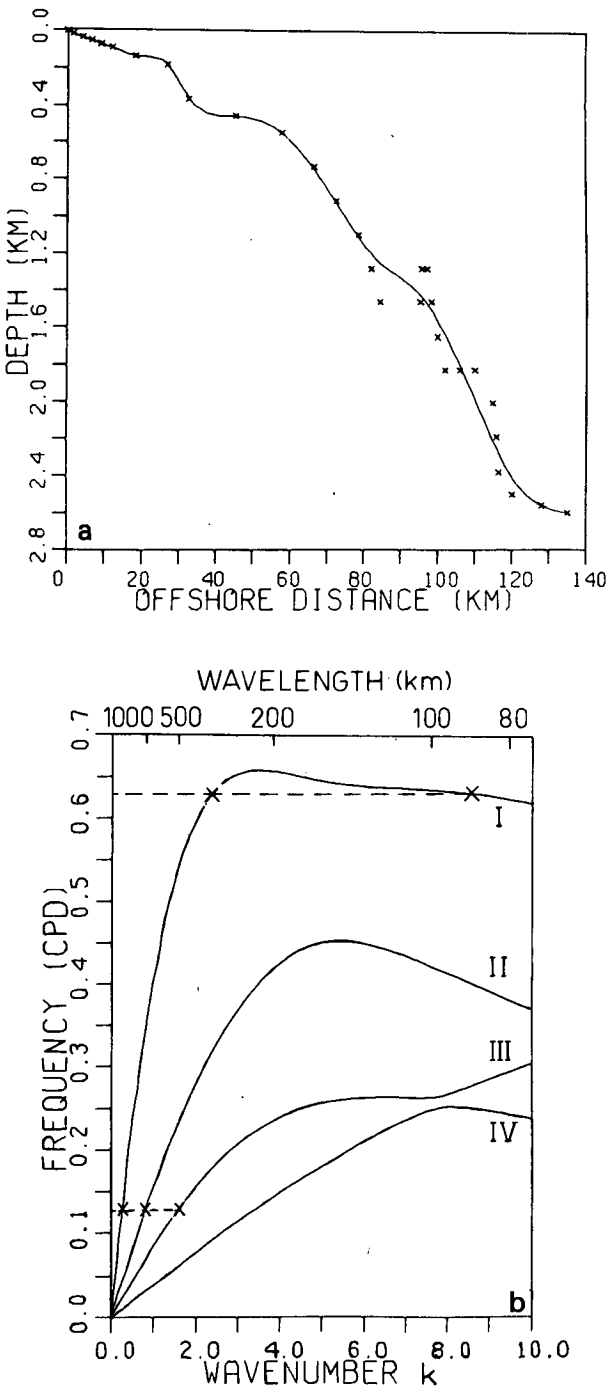

FIG. 2. (a) The topography along the cross-shelf array in Fig. 1. The crosses indicate data from contour charts. The curve is obtained by fitting spline functions to the data. (Seamounts and canyons are ignored in the fit.) (b) The shelf wave dispersion diagram obtained upon numerically integrating over the smooth curve in Fig. 2a. Only the four lowest modes (labeled by capital Roman numerals) are shown. The crosses indicate the five selected waves for which the cross-shelf structures are shown in Fig. 4. (The wavenumber k is nondimensionalized with respect to L^{-1}, where L is a length scale for the shelf/slope width, and is chosen to be 120 km. Modes 3 and 4 nearly "kissed" at $k \simeq 8$; this phenomenon is probably caused by the presence of humps on the shelf profile, as one would expect small-scale topographic perturbations to affect the short waves).

Unauthenticated | Downloaded 12/07/23 08:32 PM UTC

any shelf wave except the lowest mode long wave from sea-level data. Also, $u \ll v$ for the long waves, but becomes more comparable in magnitude for the short waves.

The corresponding anticlockwise and clockwise rotary components are displayed in Fig. 4b. We see that all the waves have $C > A$ near the coast (but right at the coast, $C = A$); i.e., from the coast to ~30 km offshore, all shelf waves have larger clockwise rotary vectors. Also note that the short wave is particularly susceptible to the influence of a topographic bump at ~20–25 km offshore.

To determine the orientation of the major axis, (2.10) requires a comparison between the magnitudes of η and η'/k. The comparison is shown in Fig. 4c, where η'/k is normalized to be unity at the coast. We see that $|\eta| \ll |\eta'/k|$ for long waves, but becomes more comparable in magnitude for short waves.

Finally, we introduce two useful quantities—P, the "polarization", and R, the "orientation" of the major axis—defined as follows:

$$P = (A - C)/(A + C), \tag{2.11}$$

$$R = (|\eta'/k| - |\eta|)/(|\eta'/k| + |\eta|). \tag{2.12}$$

P indicates the relative strength of the anticlockwise and the clockwise components. $P > 0$ when $A > C$ (overall motion anticlockwise), and $P < 0$ when $C > A$ (overall motion clockwise). Analogously, from (2.10), $R > 0$ means $\alpha = 90°$, while $R < 0$ implies $\alpha = 0°$.

Fig. 4d shows P and R as functions of the offshore distance. Two notable features are: 1) near the coast, all shelf waves have $P \leqslant 0$, since $C \geqslant A$, and 2) for all long waves, $R < 0$ occurs only in small localized regions, otherwise R is generally positive, with $\alpha = 90°$. This implies that for most of the shelf, the major axis of a current ellipse for a long shelf wave is oriented parallel to the coast.

Fig. 5 schematically illustrates the shelf wave current ellipses in the offshore x direction. The tip of the current vectors orbit around the ellipses in alternating zones of predominantly clockwise and anticlockwise motion. For any two points separated only in the alongshore y direction, their current ellipses are identical in shape; only a phase lag exists between the rotating current vectors.

We will use rotary spectral methods to detect shelf waves. Following the notation of Mooers (1973), we let

$$W(\sigma) = \int_{-\infty}^{\infty} w(t)e^{-i\sigma t}dt, \tag{2.13}$$

where

$$W(\sigma) = \begin{cases} Ae^{i\phi}, & \sigma \geqslant 0 \\ Ce^{-i\theta}, & \sigma \leqslant 0 \end{cases} \tag{2.14}$$

and A, C, ϕ, θ are functions of the angular frequency σ.

The autospectrum $S(\sigma)$ is simply $\langle A^2 \rangle$ and $\langle C^2 \rangle$, respectively, for positive and negative σ, with $\langle \cdots \rangle$ denoting a band average over neighboring frequencies. One can also calculate the coherency μ and phase $2\langle\alpha\rangle$ between the clockwise and anticlockwise components. Gonella (1972) has named μ the "stability" of the current ellipse, while $\langle\alpha\rangle$ indicates the direction of the major axis.

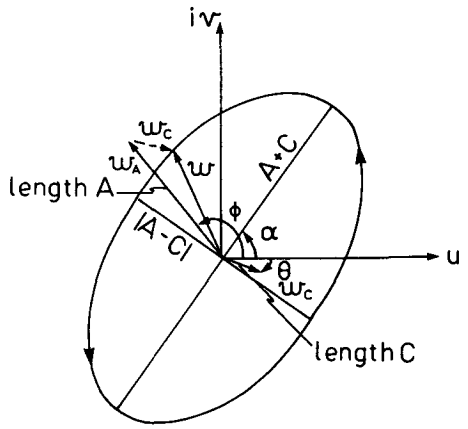

FIG. 3. The current ellipse, with rotary vectors shown at the instant $t = 0$.

With two time series, the inner cross spectrum (Mooers, 1973) gives the coherency γ^2 and the phase χ between the anticlockwise (clockwise) components of the two series, at positive (negative) frequencies. The outer cross spectrum gives the coherency λ^2 and the phase ψ between the clockwise component of the first (second) time series and the anticlockwise component of the second (first) series, at positive (negative) frequencies. The original formulas in Mooers (1973, pp. 1135–36) contain some misprints: In all the cross-terms for γ^2, μ and λ^2, the squaring should be done after the band-averaging, not before (i.e., all terms of the form $\overline{[\cdots]}^2$ should read $\overline{[\cdots]^2}$). In the formulas for λ^2 and ψ, all occurrences of ϕ and θ should be interchanged.

3. Cross-shelf modal fitting

Suppose we have a line of N stations extending offshore. Upon applying discrete Fourier transform to the current data at the nth station ($n = 1, \ldots, N$), we obtain A_n, ϕ_n, C_n and θ_n as defined in (2.14). These four quantities are functions of frequency, but let us focus on one particular frequency $|\sigma|$. Suppose that from the shelf-wave dispersion diagram, we find that M shelf waves can exist at this frequency. Their theoretical values are derived by the numerical integration scheme discussed in Section 2. Since all the stations have the same y coordinate, y in Eq. (2.4) can be set to 0. However, an arbitrary phase δ_m can be associated with the mth shelf wave ($m = 1, \ldots, M$). Thus, the rotary vectors for the mth shelf

Unauthenticated | Downloaded 12/07/23 08:32 PM UTC

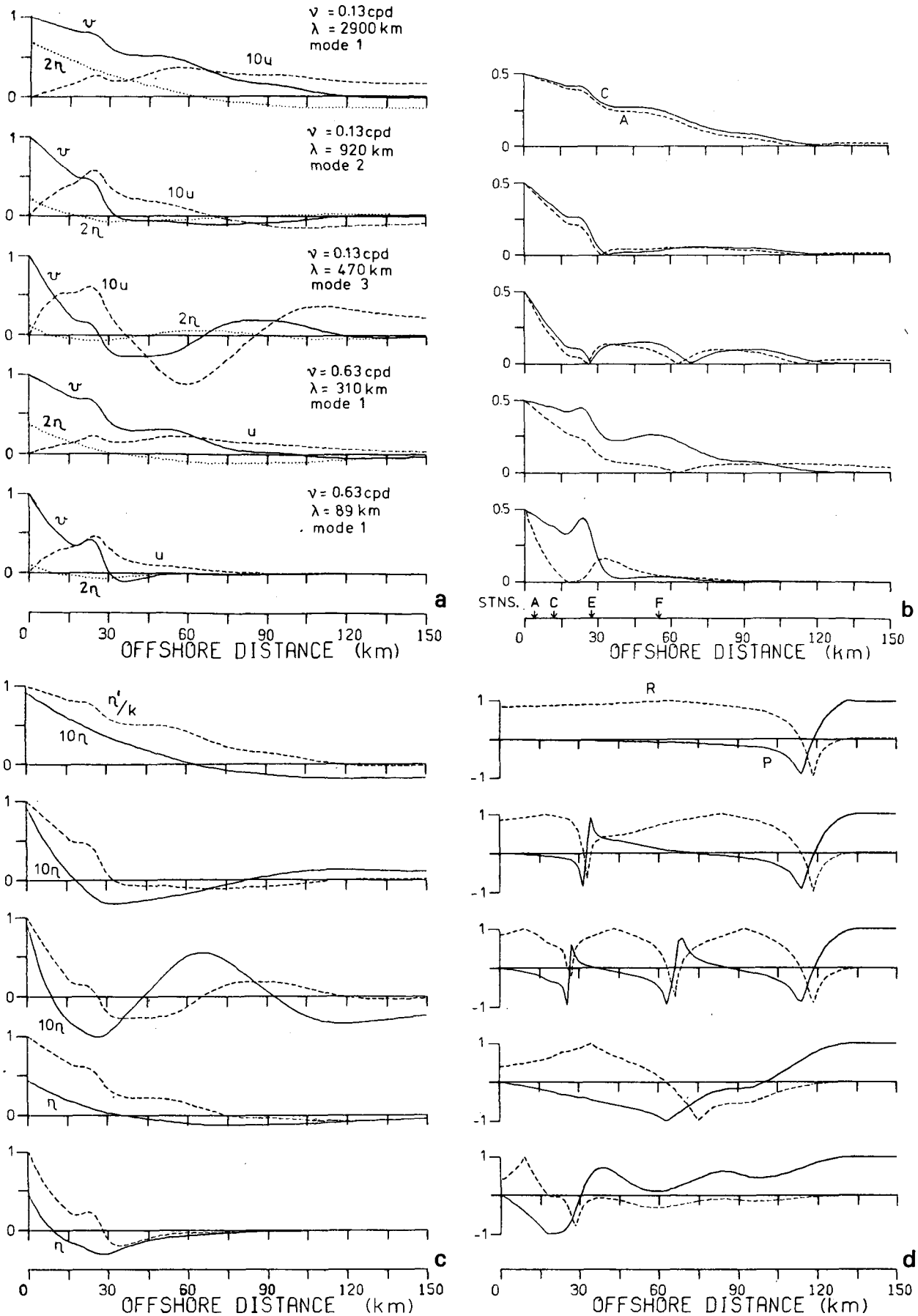

Unauthenticated | Downloaded 12/07/23 08:32 PM UTC

wave are

$$A_m e^{i\phi_m} = \tfrac{1}{2}(-u_m + iv_m)e^{i\delta_m}, \quad (3.1)$$

$$C_m e^{-i\theta_m} = \tfrac{1}{2}(u_m + iv_m)e^{-i\delta_m}. \quad (3.2)$$

Let the quantities $\tilde{A}_{nm}$, $\tilde{\phi}_{nm}$, $\tilde{C}_{nm}$, $-\tilde{\theta}_{nm}$ denote the amplitude and phase of the two rotary vectors for the mth wave evaluated at the nth station (with the tilde distinguishing these theoretical quantities from the observed ones). We next introduce the fitting function F:

$$F = \sum_{n=1}^{N} w_n\{[A_n \cos\phi_n - \sum_{m=1}^{M} a_m \tilde{A}_{nm} \cos\tilde{\phi}_{nm}(\delta_m)]^2 + [A_n \sin\phi_n - \sum_{m=1}^{M} a_m \tilde{A}_{nm} \sin\tilde{\phi}_{nm}(\delta_m)]^2 + [C_n \cos\theta_n - \sum_{m=1}^{M} a_m \tilde{C}_{nm} \cos\tilde{\theta}_{nm}(\delta_m)]^2 + [C_n \sin\theta_n - \sum_{m=1}^{M} a_m \tilde{C}_{nm} \sin\tilde{\theta}_{nm}(\delta_m)]^2\}. \quad (3.3)$$

Here, a total of M shelf waves are fitted, and associated with each wave are two parameters, the wave amplitude a_m and the phase δ_m. [It can be seen from (3.1) and (3.2) that $\tilde{\phi}_{nm}$ and $\tilde{\theta}_{nm}$ depend on δ_m, while $\tilde{A}_{nm}$ and $\tilde{C}_{nm}$ do not]. The function F is composed of four parts, corresponding to separate fits to the real and imaginary components of the anticlockwise and clockwise rotary vectors. F is minimized with respect to the parameters a_m and $\delta_m (m = 1, \ldots, M)$. The contributions from the stations can be weighed differently by adjusting the weights w_n.

In a situation where one has relatively few stations and several allowable waves, the minimum of F may occur with the waves having unreasonably large amplitudes a_m which cancel out at the stations to give a good fit. When this happens, it is better to minimize instead the function $\mathcal{F}$ where

$$\mathcal{F} = F + K[\sum_{m=1}^{M} a_m^2 \sum_{n=1}^{N} w_n \times (\tilde{A}_{nm}^2 + \tilde{C}_{nm}^2) - E_w]^2, \quad (3.4)$$

with K, a constant, and E_w, the (weighed) total "energy" observed at the stations, given by

$$E_w = \sum_{n=1}^{N} w_n (A_n^2 + C_n^2). \quad (3.5)$$

The new term on the right side of Eq. (3.4) is a "penalty" or "damping" function. With a large enough constant K, it can force the amplitudes a_m to be such that the total energy from the fit balances the observed energy. (We simply choose $K = 1$ in our fits.)

The deviation D is defined as

$$D = \mathcal{R}/E, \quad (3.6)$$

where $\mathcal{R}$ is the residual [defined identical to F in Eq. (3.3) but without the weights w_n], and E, the total "energy" observed at the stations,

$$E = \sum_{n=1}^{N} (A_n^2 + C_n^2). \quad (3.7)$$

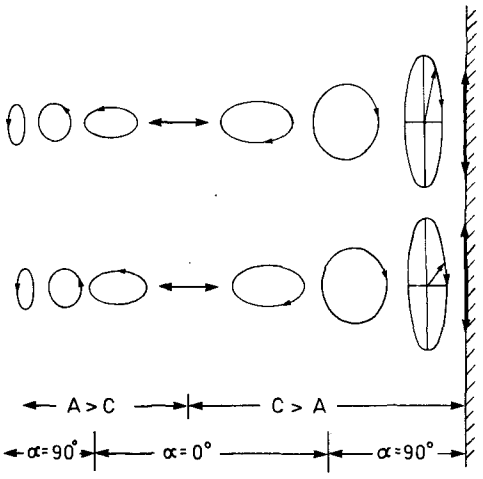

FIG. 5. Schematic diagram illustrating the current ellipses associated with a first mode shelf wave. For higher mode waves, the basic pattern is simply repeated offshore. For long waves, the zones where $\alpha = 0°$ is actually quite narrow compared to zones where $\alpha = 90°$.

4. Result of rotary spectral analysis

Before performing rotary spectral analysis on the data from the CUE-2 experiment (Fig. 1), the mean and the linear trend in the hourly current and wind data were removed.

The autospectra for the 40 m currents at Carnation and Forsythia are shown in Fig. 6. The water depth is 100 m at Carnation and 500 m at Forsythia. Notable features from the figure are: 1) Energy falls off away from the coast—consistent with the presence of coastal trapped waves. 2) The energy falls off much faster at low frequencies. For instance, at ~0.13 cpd, the ratio of the energy density at Carnation to that at Forsythia is greater than 10, while at 0.5 cpd, the ratio is ~2.4. 3) Carnation has more

FIG. 4. (a) Velocity components u, v, and sea level η for five shelf waves on the topography of Fig. 2a. These five waves are indicated by crosses in Fig. 2b. Note v is normalized to unity at the coast. (b) Clockwise and anticlockwise velocity components, C (solid curve) and A (dashed curve), for the five shelf waves. The location of the CUE-2 stations Aster, Carnation, Edelweiss and Forsythia are marked by the symbols A, C, E, and F on the offshore distance scale at the bottom. (c) A comparison between the sea-level displacement η and η'/k for the five shelf waves, with η'/k (dashed curve) normalized to unity at the coast. Note the change in scale for η for the last two waves. (d) The "polarization" P (solid curve) and the "orientation" R (dashed curve) for the five shelf waves.

Unauthenticated | Downloaded 12/07/23 08:32 PM UTC

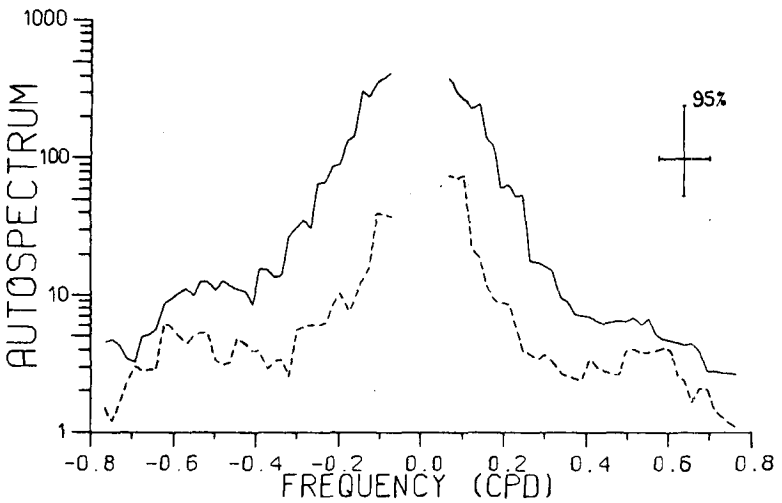

FIG. 6. Autospectra of the 40 m currents at Carnation (solid line) and at Forsythia (dashed line), in units of $(\text{cm s}^{-1})^2/\text{cpd}$. Negative (positive) frequencies for clockwise (anticlockwise) motion.

clockwise energy than anticlockwise energy at practically all frequencies. When the clockwise and anticlockwise energies are summed separately over frequencies from 0.05 to 0.8 cpd, the ratio of the total clockwise energy to anticlockwise energy is 1.35. In contrast, at Forsythia, there is considerably more anticlockwise than clockwise energy at low frequencies; but at high frequencies (>0.4 cpd) the clockwise energy again predominates. These interesting phenomena will be interpreted later. Fig. 7 shows the autospectra of the wind velocity and the adjusted sea level at Newport. The wind spectrum reveals several broad energy "humps".

The stability μ and its phase $2\langle\alpha\rangle$, are plotted for the 40 m current at Aster in Fig. 8. For high values of current stability, the phase $2\langle\alpha\rangle$ is around 180°. This means $\langle\alpha\rangle$ is ~90°, consistent with our finding in Section 2 that for most of the shelf, the major axes of shelf-wave current ellipses are oriented parallel to the coast.

The inner and outer cross-spectrum between the 40 m currents at Aster and Carnation are shown in Fig. 9. For reasonably high values of coherency, the inner phase is practically zero for all frequencies, while the outer phase is around 180°. The interpretation for the phases is as follows: Neglecting fric-

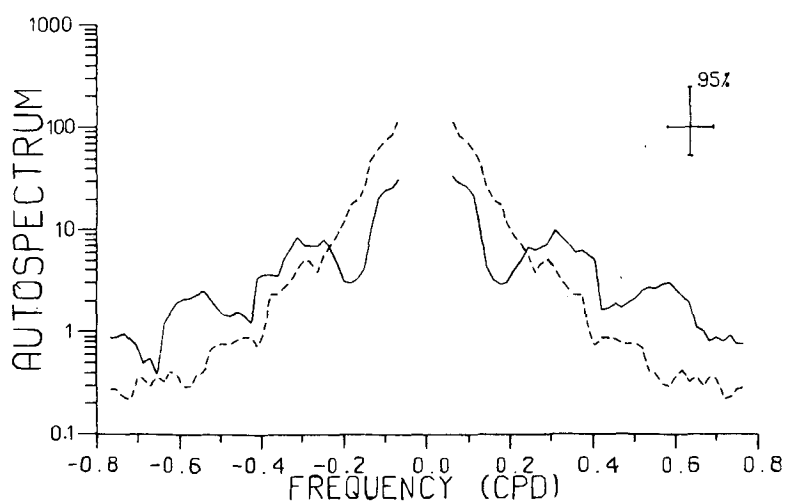

FIG. 7. Autospectra of the Newport wind (solid line) and the Newport adjusted sea level (dashed line) during CUE-2. The wind autospectrum is in units of $(\text{m s}^{-1})^2/\text{cpd}$, whereas the sea-level autospectrum is in cm^2/cpd. Since the sea level is a scalar, the two sides of the rotary spectrum are identical.

Unauthenticated | Downloaded 12/07/23 08:32 PM UTC

FIG. 8. The stability and associated phase (in degrees) for the 40 m current at Aster. The dashed line indicates the 95% significance level according to Groves and Hannan (1968).

tional and topographic effects, propagating shelf waves should manifest $\phi_1 = \phi_2$ and $\theta_1 = \theta_2$ for the phases observed at two stations separated only in the cross-shelf direction and close enough to shore (so that no shelf-wave nodes occur between them). However, as the major axes of the current ellipses are oriented alongshore ($\alpha_j = 90°$, and $\phi_j - \theta_j = 2\alpha_j = 180°$, $j = 1, 2$), the result is

$$\phi_1 - \theta_1 = \phi_2 - \theta_2 = \phi_1 - \theta_2 = \phi_2 - \theta_1 = 180°. \quad (4.1)$$

It follows from the formulas in Mooers (1973) that the inner phase should be 0° while the outer phase should be 180°, as is indeed observed. [Brink and Allen (1978) showed that bottom friction can introduce a cross-shelf phase lag. A small lag of 5–10° between Aster and Carnation (Aster leading) appeared to be present in Fig. 9 at low frequencies].

Next, we examine cross-spectra between stations separated in the alongshore direction. Fig. 10a shows the inner cross-spectrum between the 40 m currents at Carnation and at Poinsettia, two stations separated 60 km alongshore. Wang (1980) investigated numerically the behavior of shelf waves propagating over bumps and narrowing shelves, and found rather complex phase propagation due to reflection and diffraction. However, downstream away from the topographic disturbance, the constant phase lines again aligned themselves perpendicular to the depth contours. This topographic steering or refraction effect is well illustrated in the scatter diagram of Kundu and Allen (1976, p. 186). Since the depth contours

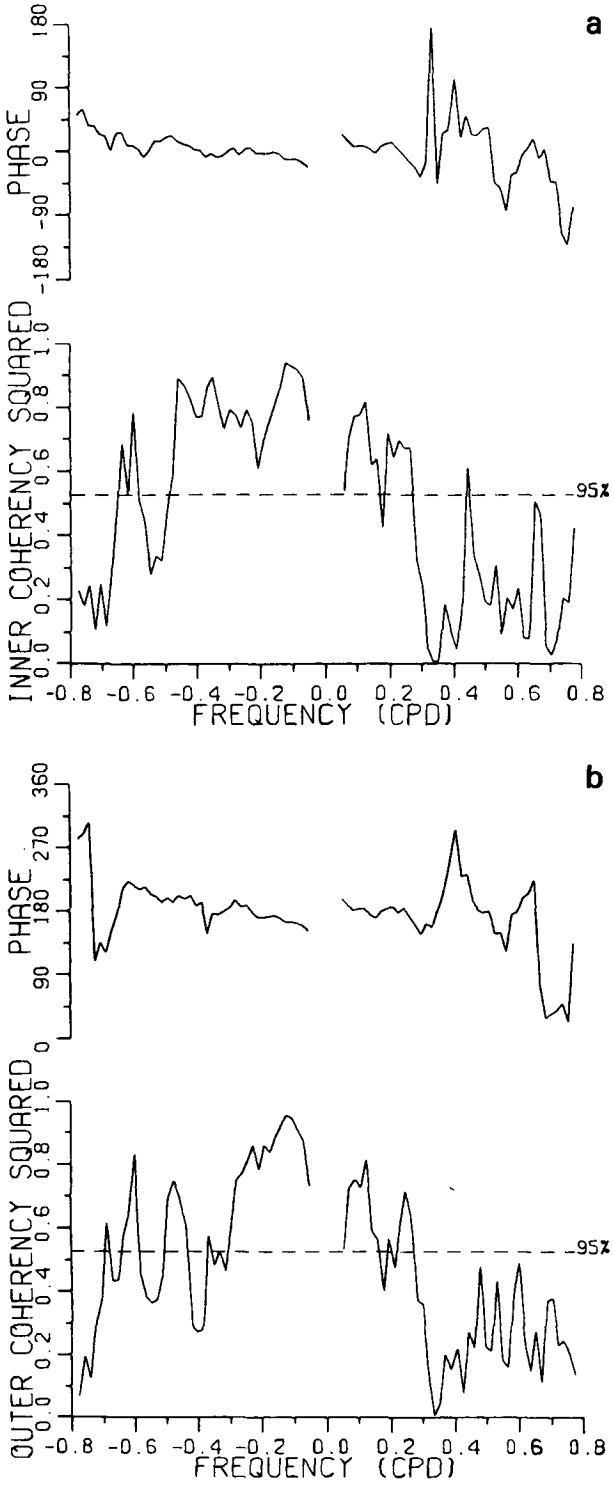

FIG. 9. (a) The inner cross-spectrum and (b) the outer cross-spectrum between the 40 m currents at Aster and Carnation.

Unauthenticated | Downloaded 12/07/23 08:32 PM UTC

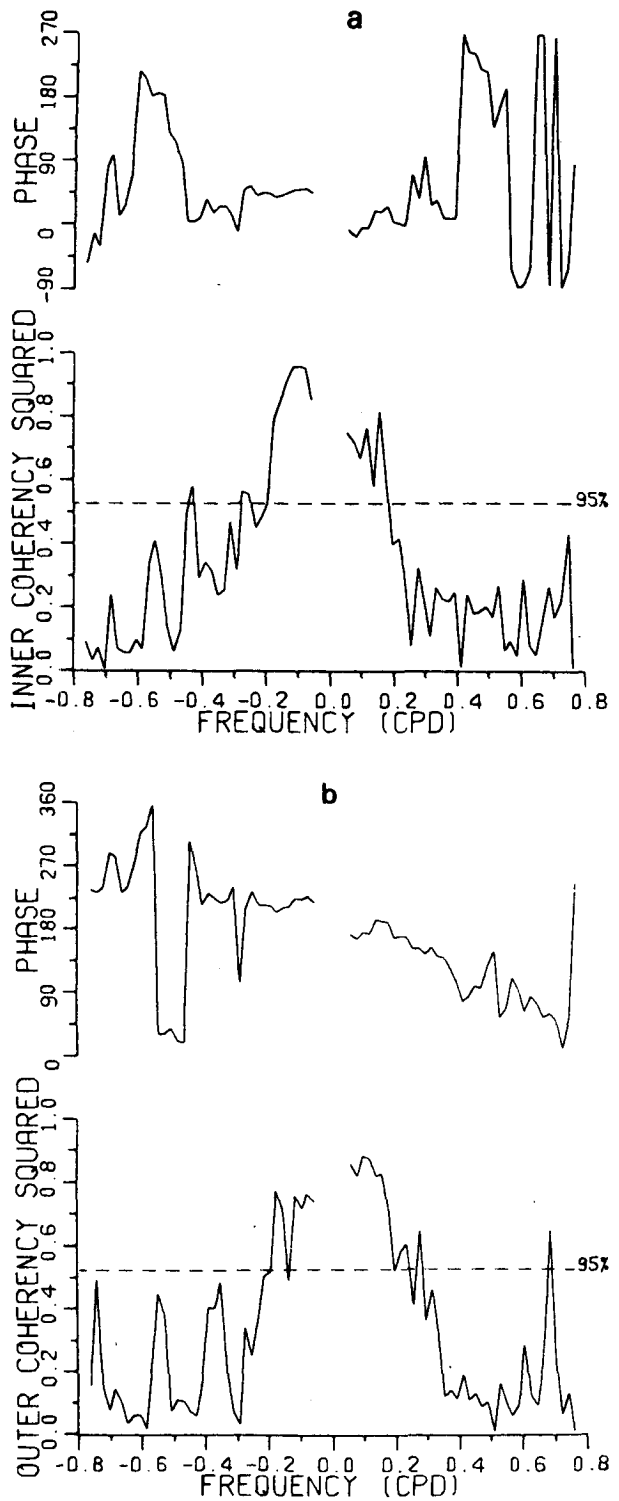

FIG. 10. (a) The inner cross-spectrum and (b) the outer cross-spectrum between the 40 m currents at Carnation and Poinsettia.

at Poinsettia are tilted by ~35° from those at Carnation (see Fig. 1), the second time series w_2 would be multiplied by an extra phase factor $\exp(-i\delta_T)$, assuming the constant phase lines align themselves perpendicular to the depth contours. From Eqs. (2.13) and (2.14), it can be seen that $\phi_2 \rightarrow \phi_2 - \delta_T$ and $\theta_2 \rightarrow \theta_2 + \delta_T$. This causes the inner phase to shift by the amount δ_T for both positive and negative values of σ. Thus, the observed inner-phase (and similarly, the outer-phase) would be positively shifted by ~35° due to the changing topography.

If there is an alongshore phase lag δ_w due to a propagating shelf wave (with the convention δ_w positive when the wave is traveling northward, i.e. northern station lags southern station), the observed inner-phase χ will be

$$\chi_- = \delta_w + \delta_T, \quad \chi_+ = -\delta_w + \delta_T, \qquad (4.2)$$

where χ_- is the inner-phase for negative σ (clockwise motion) and χ_+ for positive σ (anticlockwise) (i.e., in the absence of δ_T, a northward propagating shelf wave would manifest itself by showing a positive value for χ_- and a negative value of the same magnitude for χ_+). δ_w and δ_T can be obtained easily from

$$\delta_w = (\chi_- - \chi_+)/2, \quad \delta_T = (\chi_- + \chi_+)/2. \qquad (4.3)$$

Fig. 10a shows that at low frequencies, the inner phase is slightly above 35° for negative frequencies and slightly below 35° for positive frequencies, consistent with northward propagating long waves with corresponding small δ_w. For the 0.13 cpd peak, with 95% confidence, $\delta_T = 26° \pm 10°$ (quite close to the 35° expected from the orientation of the contours), and $\delta_w = 20°$. $\delta_w = 20°$ translates into a northward propagating wave with a wavelength of 1080 km, and a wavenumber of 0.70 on the dispersion diagram Fig. 2b. One sees that a frequency of 0.13 cpd and a wavenumber of 0.70 fit very well to a second-mode shelf wave. (When comparing phase speeds, the observed value is 140 km day^{-1}, while the theoretical value is 130 km day^{-1}). This agrees with Kundu and Allen (1976), where from the lag time of maximum correlation (without spectral decomposition) between currents at alongshore stations, a northward propagation speed consistent with second mode nondispersive long shelf waves was found.

Fig. 10b shows the corresponding outer cross-spectrum between the 40 m currents at Carnation and Poinsettia. At low frequencies, the outer phase lies close to 180° + δ_T, indicating small alongshore phase shift (δ_w) and hence long waves.

Fig. 11 shows the inner cross-spectrum between the 40 m current at Poinsettia and the wind at Newport. We find significant coherency (especially for clockwise frequencies) between wind and current at frequencies below 0.4 cpd. The higher coherency bands in Fig. 11 generally correspond to the "humps" in the wind autospectrum (Fig. 7). The phase shows the wind to lead the current slightly; however, the lead increases to over 90° at ~ −0.5 cpd.

Unauthenticated | Downloaded 12/07/23 08:32 PM UTC

5. Results of cross-shelf modal analysis

We next proceed to perform cross-shelf modal fitting. Four stations, Aster (20 m), Carnation (40 m), Edelweiss (80 m) and Forsythia (40 m) are used. (As the water depth is only 50 m at Aster, the 20 m current record is chosen; while at Edelweiss, the 40 m current record is defective, so the 80 m record is used instead).

Upon Fourier transforming the current data, the quantities A, C, ϕ and θ from Eq. (2.14) are obtained as functions of frequency. (The time series must all have the same starting time. Otherwise, the phase of one time series would be shifted by $|\sigma|t$ with respect to another, where t is the difference in the starting times. As the record for Edelweiss started much later than the others, the phases for Edelweiss had to be corrected by $|\sigma|t$). For higher statistical significance, these quantities are band-averaged over neighboring frequencies using the formulas

$$\left.\begin{aligned} A_n &= \langle A^2\rangle^{1/2} \\ \phi_n &= \arg(\langle A\cos\phi\rangle + i\langle A\sin\phi\rangle) \\ C_n &= \langle C^2\rangle^{1/2} \\ \theta_n &= \arg(\langle C\cos\theta\rangle - i\langle C\sin\theta\rangle) \end{aligned}\right\}, \quad (5.1)$$

where $\langle\cdots\rangle$ denote band-averaging, and the subscript n has been added to the new quantities (n labels the quantity from the nth station). Data for Aster, Carnation and Forsythia are averaged over five frequency bands, but for Edelweiss (due to its shorter record) only over three bands.

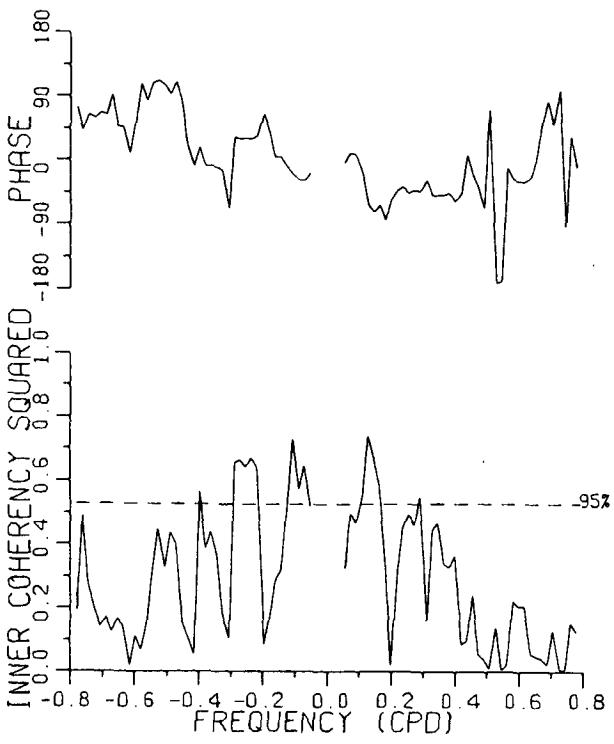

FIG. 11. The inner cross-spectrum between the 40 m current at Poinsettia and the wind at Newport.

TABLE 1. Cross-shelf modal fitting at selected frequencies. The nondimensional wavenumber k associated with each mode at a particular frequency is obtained from Fig. 2b, with λ the corresponding wavelength. The last column indicates the closeness of fit, with a small deviation value implying good fit at that frequency. The second last column gives the relative portion of energy contributed by the particular mode, when more than one mode are fitted.

Freq. (cpd)	Mode	k	λ (km)	$E_m/\Sigma E_m$	Deviation
0.13	1	0.26	2900	0.17	0.05
	2	0.82	920	0.70	
	3	1.6	470	0.00	
	4	3.5	210	0.14	
0.30	1	0.67	1100	0.01	0.09
	2	2.2	340	0.91	
	3	9.7	78	0.08	
0.43	1	1.1	690	0.05	0.36
	2	4.2	180	0.72	
	2	7.2	100	0.23	
0.53	1	1.5	502	—	0.33

The following frequencies are selected for modal fitting: 0.13, 0.30, 0.43 and 0.53 cpd. The first four columns of Table 1 list the possible shelf waves at these selected frequencies. The entries in column 3 are obtained from the intersections on the dispersion diagram (Fig. 2b) between horizontal lines drawn at the selected frequencies and the dispersion curves. Possible contributions from waves with $k > 10$ ($\lambda < 75$ km) have been neglected. Note that the second mode actually contributed two waves of different wavelengths at 0.43 cpd.

The fitting was performed by minimizing F in Eq. (3.3) for each of the selected frequencies. Since the offshore stations have much smaller wave amplitudes than the nearshore stations, the weights w_n have to be increased for the offshore stations. Also, the data from Edelweiss were only used for the fitting at 0.13 cpd; for the other frequencies, only three stations were employed. Recall that each station supplies four numbers (A_n, C_n, ϕ_n, θ_n), and each shelf wave introduces two parameters (a_m and δ_m) to be determined from the fitting. For instance, for the 0.43 cpd frequency, we have three stations supplying 12 numbers and three shelf waves with six parameters to be fitted. The results of the fitting are shown in the last columns of Table 1.

The entry $E_m/\Sigma E_m$ indicates the relative energy contribution of the mth wave in the fit. E_m, the energy of the mth wave ($m = 1, \ldots, M$), is defined as

$$E_m = \sum_{n=1}^{N} a_m^2(\tilde{A}_{nm}^2 + \tilde{C}_{nm}^2) \quad (5.2)$$

Unauthenticated | Downloaded 12/07/23 08:32 PM UTC

and ΣE_m, the total energy of the fit, is the sum of the E_m's. For the frequencies 0.13 and 0.43 cpd, the fits were obtained by minimizing the function $\mathcal{F}$ of (3.4), instead of F. (When F was used, severe "overfitting" resulted at these frequencies, i.e. ΣE_m becomes much larger than E, the total observed energy at the stations).

The deviation D, defined in Eq. (3.6) as the ratio of the residual after the fit to the total observed energy, is small when the fit is good. From the deviation values in Table 1, we see that the fit is excellent at 0.13 cpd, good at 0.30 cpd, fair at 0.43 and 0.53 cpd.

The fits at 0.13, 0.30 and 0.43 cpd reveal that at low frequencies the cross-shelf structure is dominated by the second mode, in agreement with the alongshore phase lag measurements mentioned earlier, which gave the phase speed of the second mode shelf wave. This is also the first time a strong signal (at 0.13 cpd) has been unambiguously identified as a shelf wave from alongshore *and* cross-shelf observations. The deviation D increases with the frequency, indicating a decrease in the signal to noise ratio as the frequency increases. This is not surprising, as the cross-spectra in the previous section showed generally lower coherency for the higher-frequency peaks.

To check the reliability of the fit at 0.13 cpd, six trials using random data were performed. The amplitudes A and C were uniformly distributed between 0 and 1, and the phases between 0 and 360°. The six trials yielded a mean value of 0.55 for D, with a standard error of ± 0.11.

6. Limitations and extentions of the cross-shelf modal fitting technique

We now turn back to the current autospectra in Fig. 6, and interpret the salient features pointed out in the second paragraph of Section 4. We have noted that the ratio of energy at Carnation and at Forsythia was greater than 10 at lower frequencies, and around 2–3 at higher frequencies. This rapid energy falloff at low frequencies is not surprising since Fig. 4b shows the second mode to fall off much faster than the first mode. At frequencies above 0.45 cpd, Fig. 2b shows that only the first mode can be excited, hence the much slower falloff at higher frequencies.

Also, we have noted from Fig. 6 that at low frequencies, Forsythia has more anticlockwise energy than clockwise energy, the reverse of the situation at Carnation. In Fig. 4b, the second mode at 0.13 cpd indeed has $A > C$ at Forsythia, but $C > A$ at Carnation. In fact, these good agreements are to be expected, since our cross-shelf modal analysis has already shown the second mode to be an excellent fit to the observed current fluctuations.

Though powerful, the cross-shelf modal fitting technique has its limitations: 1) It works well only when the width and shape of the continental shelf are not changing drastically in the alongshore direction. 2) It is unsuitable for detecting short shelf waves, since these are far more sensitive to topographic perturbations than the long waves. For instance, it is not useful for detecting the short shelf waves arising from resonant triad interactions as described in Hsieh and Mysak (1980). 3) So far, no attempt has been made to incorporate stratification, which also tends to affect the short waves more than the long waves.

Surprisingly, the cross-shelf fitting does not separate out free waves from wind-forced waves. In the linear, non-dispersive, long-wave treatment of Gill and Schumann (1974), the forced problem

$$\mathcal{L}\psi = \mathcal{F} \tag{6.1}$$

(where $\mathcal{L}$ is a linear differential operator, ψ the stream function and $\mathcal{F}$ the wind forcing), is expanded in terms of the eigenfunctions of the free-wave problem, i.e.,

$$\psi = \sum_n \phi_n(y, t)F_n(x), \tag{6.2}$$

where F_n are the cross-shelf eigenfunctions of the unforced problem, n being the mode number. For wind systems traveling alongshore, the solution for ϕ_n consists of two waves, one which propagates at the nth mode free-wave phase speed, and one, the forced wave, at the alongshore phase speed of the wind system. Since the cross-shelf structure of the forced wave can be expanded in terms of the free-wave eigenfunctions F_n, the cross-shelf fitting of free-wave eigenfunctions only indicates how the total kinetic energy, from both free and forced waves, is distributed among the eigenmodes.

Though the modal fitting technique by itself does not distinguish between energy contributions from free and forced waves, the conclusion that the current fluctuations during that summer were essentially due to a second mode shelf wave remains firm, for the following reasons: 1) Wang and Mooers (1977, Fig. 6b) found that during that summer, atmospheric pressure propagated northward along the Oregon coast at 820 km day^{-1}, many times faster than the observed current phase speed (which agreed extremely well with the phase speed of the second mode shelf wave). If a strong forced wave were present together with the shelf wave, the observed current phase speed would have been much higher. 2) With the atmospheric system traveling much faster than the shelf waves, the linear forcing theory of Gill and Schumann (1974) predicts a non-resonant response consisting of a forced wave (with its energy broadly distributed among the eigenmodes, decreasing with increasing mode number) and free waves (also broadly distributed). Instead, our cross-shelf fitting found that the energy was essentially all concen-

Unauthenticated | Downloaded 12/07/23 08:32 PM UTC

trated in the second mode, in contradiction to the theory.

This does not necessarily imply that the shelf wave was unrelated to the wind system. In fact, the sharp concentration of energy into one mode strongly suggests some yet unknown wind-current resonant mechanism at work. This difficult and controversial topic is discussed in Hsieh (1982, Section 4).

The fitting technique has obvious extensions:

1) Suppose we now have J cross-shelf lines of moorings separated alongshore, with the jth line ($j = 1, \ldots, J$) containing N_j stations spread across the shelf. A dispersion diagram can be computed for each line. For a particular frequency, we can select M shelf waves for fitting. These have (dimensional) wavenumbers k_{mj} ($m = 1, \ldots, M$) on the jth dispersion diagram ($j = 1, \ldots, J$). The fitting function F generalizes from (3.3) to

$$F = \sum_{j=1}^{J} \sum_{n=1}^{N_j} w_{nj}\{[A_{nj}\cos\phi_{nj} - \sum_{m=1}^{M} a_m \tilde{A}_{nmj}\cos\tilde{\phi}_{nmj}(\delta_m)]^2 + \cdots\}, \quad (6.3)$$

where the last three terms of (3.3) are extended similarly as the first term. If ΔL_j is the distance separating the jth and the $(j+1)$th lines, then alongshore phase lags are taken into account by setting

$$\begin{pmatrix}\tilde{\phi}_{nmj+1}\\ \tilde{\theta}_{nmj+1}\end{pmatrix} = \begin{pmatrix}\tilde{\phi}_{nmj}\\ \tilde{\theta}_{nmj}\end{pmatrix} - \frac{\Delta L_j(k_{mj} + k_{mj+1})}{2}\begin{pmatrix}1\\ 1\end{pmatrix} \text{ (radians)}. \quad (6.4)$$

By incorporating alongshore phase lags into our fit, we are no longer fitting only cross-shelf eigenmodes, but the full free-wave model. If the wavenumber k_w of the wind system is also known, the forced wave can be included in the fit as well, and a distinction between free and forced waves may be possible.

2) The fitting can be generalized to three dimensions. If stratification is known, the current ellipses at different depths can be computed, and fitted to the observed current ellipses at various depths, thus allowing us to study both the barotropic and baroclinic motions.

3) This technique can probably be extended to other types of waves, e.g. edge waves on a beach.

7. Problems with detecting shelf waves from sea-level data

It has long been realized that the amount of potential energy associated with the sea-level displacements of a shelf wave is very small compared to the amount of kinetic energy associated with the horizontal current oscillations of the shelf wave. The smallness of r, the ratio of potential to horizontal kinetic energy of the wave, does not by itself rule out sea level as an indicator for shelf waves (except that the shelf wave signals might be masked by other types of waves with much larger r, as discussed below). The problem lies not in the absolute size of r, but in the relative size of r (r changes substantially between different shelf-wave modes, diminishing as the mode number increases). For instance, at 0.13 cpd, Fig. 4a shows that for the same alongshore velocity at the coast, the corresponding sea-level displacement of the first mode is larger than that of the second mode by more than a factor of 3. When one computes auto- or cross-spectra of sea levels, this factor is squared, resulting in the first mode appearing 10 times stronger than the second. This intrinsic bias for the lowest mode is unfortunately present in previous studies which used sea-level data for shelf-wave detection.

Table 1 shows that at 0.13 cpd, the current energy of the second mode dominated over that of the first by a ratio of 4:1. Yet, due to the factor of 10 bias, we expect the sea-level auto- or cross-spectra to be dominated by the first mode. This explains the peculiar phenomenon resulting from the separate observations of Kundu and Allen (1976), and Wang and Mooers (1977, Fig. 6b). While both studies employed data from the Oregon shelf during the summer of 1973, the former, using *current* data, deduced an alongshore propagation speed of 120 km day^{-1}, consistent with the second mode shelf wave, while the latter, using *sea-level* data, obtained a phase speed of 460 km day^{-1}, comparable to that of the first mode.

Cutchin and Smith (1973) tried to detect a third mode shelf wave [predicted by the zero group speed resonance mechanism of Buchwald and Adams (1968)], from coastal sea-level data without success. Fig. 4a shows that at 0.13 cpd frequency, the coastal sea-level displacement of the first mode is six times as large as that of the third mode, resulting in a bias factor of $\sim$36 in the auto- or cross-spectra. In recent years, scattering theories have shown that topographic irregularities can transfer energy between shelf waves of the *same frequency* but different wavenumbers (see, e.g., Mysak, 1980, Section 6). Hence, if a third mode wave is present, topographic irregularities may scatter some of its energy into the first mode at the same frequency. With the bias factor of $\sim$36, it would be very difficult to detect from sea-level data the larger alongshore phase lag associated with the third mode short wave, even if it had been present.

In fact, obtaining alongshore phase lags that were substantially smaller than the theoretical values (or equivalently, finding phase speeds that were too large) seemed to be a common problem encountered when using sea-level data to detect shelf waves. In

Unauthenticated | Downloaded 12/07/23 08:32 PM UTC

extreme cases, Mysak and Hamon (1969) and Brooks (1978) all found alongshore phase lags that were about a factor of 3 smaller than expected, while Brooks and Mooers (1977) found their phase lags and corresponding phase speeds to be off by a factor of 10.

A possible source of contamination is the Kelvin wave. At sub-tidal frequencies, the Kelvin wave has very long wavelength, (of the order of 10^5 km), and hence is not usually excited. However, if a shelf wave is excited at a certain frequency, topographic irregularities can probably scatter a tiny fraction of its energy into a Kelvin wave of the same frequency. Cutchin and Smith (1973, Fig. 7) showed that at the coast, the associated sea-level displacement of the Kelvin wave was ~40 times that of the first mode shelf wave. In other words, on the shelf, the ratio of potential to horizontal kinetic energy for the Kelvin wave is ~1600 times that of the first mode shelf wave. Thus, even a small input of energy (by whatever mechanism) into the Kelvin mode could seriously contaminate the sea-level data (but not the current data).

Suppose the sea-level η is now composed of a shelf wave and a Kelvin wave of the same frequency, but different wavenumbers k_1 and k_0, respectively,

$$\eta = a\cos(k_1 y - \omega t) + b\cos(\delta + k_0 y - \omega t), \quad (7.1)$$

with δ an arbitrary phase. Depending on the amplitudes a and b, the resulting propagation speed c will lie somewhere between ω/k_1 and ω/k_0. In the special case $a = b$, (7.1) can be written as

$$\eta = 2a\cos\left[-\frac{\delta}{2} + \frac{(k_1 - k_0)}{2}y\right] \times \cos\left[\frac{\delta}{2} + \frac{(k_1 + k_0)}{2}y - \omega t\right]. \quad (7.2)$$

The propagation speed c is $2\omega/(k_1 + k_0)$. Since $k_0 \ll k_1$, $c \approx 2\omega/k_1$, i.e. twice the shelf-wave phase speed. Thus, contamination by the Kelvin wave may be an explanation for the frequent detection of unexpectedly high phase speeds in the observations of shelf waves from sea-level data.

The presence of a forced wave can also increase the observed phase speed [see Gill and Schumann (1974), Eqs. (6.2), (7.6) and (7.8)]. However, unlike Kelvin wave contamination, the forced wave should affect both current and sea-level observations.

8. Summary

The sea level is not a reliable indicator for shelf waves, which are primarily horizontal current oscillations. The ratio of potential to horizontal kinetic energy is not only very small for shelf waves, but also highly modal-dependent. At a given frequency, this ratio decreases with increasing mode number. Thus, an intrinsic bias for the lowest mode is present when using sea-level data for shelf-wave detection.

Turning to horizontal current oscillations, we have noted that the cross-shelf dimension of continental shelf waves contains rich structures—alternating zones of predominantly clockwise and anticlockwise motions, modal-dependent energy falloff rates, varying shapes and orientations of the current ellipses. As these structures are unique to each mode, they can be used to accurately identify the excited modes in the observed current fluctuations.

The basic observational procedure used in this paper is as follows:

1) From the cross-shelf topography, the shelf wave dispersion diagram and the cross-shelf structures of various modes are obtained by numerical integration.

2) Rotary spectral analysis of currents from stations separated in the alongshore and cross-shelf directions are performed.

3) At a chosen frequency, the theoretical current ellipses of several modes can be fitted by least-squares to the observed current ellipses, thereby showing how the current energy is distributed among the eigenmodes.

This procedure was applied to Oregon shelf data from the summer of 1973. Upon performing cross-shelf modal fitting at selected frequencies, we found that below 0.45 cpd, the energy of the current fluctuations on the shelf was sharply concentrated in the second eigenmode. Furthermore, the alongshore propagation speed also agreed extremely well with the theoretical second mode phase speed. Thus, the presence of a second mode shelf wave off the coast of Oregon during the summer of 1973 is firmly established.

Acknowledgments. I thank Dr. A. Huyer of Oregon State University at Corvallis for generously supplying the Oregon shelf data, and my doctoral dissertation supervisor, Professor L. A. Mysak, for his encouragement and support. This work was supported by the Natural Sciences and Engineering Research Council of Canada. Dr. A. E. Gill provided helpful discussions during the revision of this paper.

REFERENCES

Brink, K. H., and J. S. Allen, 1978: On the effect of bottom friction on barotropic motion over the continental shelf. *J. Phys. Oceanogr.*, **8**, 919–922.

Brooks, D. A., 1978: Subtidal sea level fluctuations and their relation to atmospheric forcing along the Carolina coast. *J. Phys. Oceanogr.*, **8**, 481–493.

Brooks, D. A., and C. N. K. Mooers, 1977: Wind forced continental shelf waves in the Florida Current. *J. Geophys. Res.*, **82**, 2569–2576.

Buchwald, V. T., and J. K. Adams, 1968: The propagation of continental shelf waves. *Proc. Roy. Soc. London*, **A305**, 235–250.

Caldwell, D. R., and M. S. Longuet-Higgins, 1971: The experi-

Unauthenticated | Downloaded 12/07/23 08:32 PM UTC

mental generation of double Kelvin waves. *Proc. Roy. Soc. London*, **A326,** 39–52.

Cutchin, D. L., and R. L. Smith, 1973: Continental shelf waves: Low frequency variations in sea level and currents over the Oregon continental shelf. *J. Phys. Oceanogr.*, **3,** 73–82.

Gill, A. E., and E. H. Schumann, 1974: The generation of long shelf waves by the wind. *J. Phys. Oceanogr.*, **4,** 83–90.

Gonella, J., 1972: A rotary-component method for analyzing meteorological and oceanographic vector time series. *Deep-Sea Res.*, **19,** 833–846.

Groves, G. W., and E. J. Hannan, 1968: Time series regression of sea level on weather. *Rev. Geophys.*, **6,** 129–174.

Hamon, B. V., 1962: The spectrums of mean sea level at Sydney, Coff's Harbour, and Lord Howe Island. *J. Geophys. Res.*, **67,** 5147–5155. (Correction, *J. Geophys. Res.*, **68,** 4635).

Hsieh, W. W., 1981: Resonant interactions between continental shelf waves. Ph.D. thesis, University of British Columbia, 128 pp.

——, 1982: Observations of continental shelf waves off Oregon and Washington. *J. Phys. Oceanogr.,* **12,** (in press).

——, and L. A. Mysak, 1980: Resonant interactions between shelf waves, with applications to the Oregon shelf. *J. Phys. Oceanogr.*, **10,** 1729–1741.

Huyer, A. B., B. M. Hickey, J. D. Smith, R. L. Smith and R. D. Pillsbury, 1975: Alongshore coherence at low frequency in currents observed over the continental shelf off Oregon and Washington. *J. Geophys. Res.*, **80,** 3495–3505.

——, R. L. Smith and E. J. Sobey, 1978: Seasonal differences in low-frequency current fluctuations over the Oregon shelf. *J. Geophys. Res.*, **83,** 5077–89.

Kundu, P. K., and J. S. Allen, 1976: Some three-dimensional characteristics of low-frequency current fluctuations near the Oregon coast. *J. Phys. Oceanogr.*, **6,** 181–199.

——, —— and R. L. Smith, 1975: Modal decomposition of the velocity field near the Oregon coast. *J. Phys. Oceanogr.*, **5,** 683–704.

Mooers, C. N. K., 1973: A technique for the cross spectrum analysis of pairs of complex-valued time series, with emphasis on properties of polarized components and rotational invariants. *Deep-Sea Res.*, **20,** 1129–1141.

——, and R. L. Smith, 1968: Continental shelf waves off Oregon. *J. Geophys. Res.*, **73,** 549–557.

Mysak, L. A., 1980: Recent advances in shelf wave dynamics. *Rev. Geophys. Space Phys.*, **18,** 211–241.

——, and B. V. Hamon, 1969: Low-frequency sea level behavior and continental shelf waves off North Carolina. *J. Geophys. Res.*, **74,** 1397–1405.

Osmer, S. R., and A. Huyer, 1978: Variations in the alongshore correlation of sea level along the west coast of North America. *J. Geophys. Res.*, **83,** 1921–27.

Pillsbury, R. D., J. S. Bottero, R. E. Still and W. E. Gilbert, 1974: A compilation of observations from moored current meters: Vol. VII; Oregon continental shelf, July–August 1973. Ref. 74-7, School of Oceanography, Oregon State University, Corvallis, 87 pp.

Schott, F., and W. Düing, 1976: Continental shelf waves in the Florida Straits. *J. Phys. Oceanogr.*, **6,** 451–460.

Wang, D.-P., 1980: Diffraction of continental shelf waves by irregular alongshore geometry. *J. Phys. Oceanogr.*, **10,** 1187–1199.

——, and C. N. K. Mooers, 1977: Long coastal-trapped waves off the west coast of the United States, summer 1973. *J. Phys. Oceanogr.*, **7,** 856–864.

Unauthenticated | Downloaded 12/07/23 08:32 PM UTC